

# Effect of Molecular Position and Orientation on Adsorbate-Induced Shifts of Plasmon Resonances

Chhayly Tang<sup>1,\*</sup>, Baptiste Auguié<sup>1</sup>, and Eric C. Le Ru<sup>1†</sup>

<sup>1</sup>*The MacDiarmid Institute for Advanced Materials and Nanotechnology and The School of Chemical and Physical Sciences, Victoria University of Wellington, PO Box 600, Wellington 6140, New Zealand*

(Dated: October 13, 2022)

Localized surface plasmon resonances (LSPRs) of metallic nanoparticles are affected by their surrounding and in particular by the presence of adsorbed molecules on their surface. This effect is central to their application in LSPR sensing. We here investigate how the adsorbed molecule orientation on the surface and position, notably with respect to an electromagnetic hot-spot, affect the amplitude of the resonance shift, and therefore the LSPR sensing sensitivity. We use a recently developed effective anisotropic dielectric function describing a homogeneous shell of adsorbed molecules combined with anisotropic Mie theory calculations for core-shell spherical systems or finite-element modelling for non-spherical or partial shell configurations. We show that the induced plasmon resonance shift per molecule is strongly correlated with the near-field enhancement experienced by the adsorbed molecules. Molecules with their main optical axis perpendicular to the surface and those located at hot-spots can therefore induce much larger resonance shift, by at least one order of magnitude. This work suggests that large improvements in LSPR sensing sensitivity could be achieved with new schemes including targeted adsorption at hot-spots with carefully engineered molecular orientation.

Keywords: Plasmon Resonance, Localized Surface Plasmon Resonance, Plexcitonics, Metallic Nanoparticles, Optical Properties

The interaction between molecules adsorbed on metallic nanoparticles (NPs) and localized surface plasmon resonances (LSPRs) is central to many fundamental studies and applications, including LSPR sensing,<sup>1–6</sup> surface-enhanced Raman spectroscopy (SERS),<sup>7,8</sup> surface-enhanced Fluorescence (SEF),<sup>8–11</sup> and the study of weak<sup>12–17</sup> and strong<sup>18–21</sup> coupling between molecular and plasmon resonances (PRs). It is well accepted that the adsorbed molecules affect the plasmon resonance, for example inducing shifts,<sup>22–25</sup> which is the basis for applications in LSPR sensing. Conversely, it was recently demonstrated that the metal surface also has an effect on the molecular resonance.<sup>17,26</sup> When the plasmon and molecular resonance overlap (for example for dyes on metal NPs),<sup>13–16,27–29</sup> these mutual interactions can no longer be clearly separated and should be treated as a single plasmon/molecule system, in particular in the strong coupling regime.<sup>18–21</sup>

There are two main general approaches to theoretically study the optical properties of such systems. In the first one, the light scattering problem is solved for the metallic nanoparticle only. The optical response of the adsorbed molecules can then be derived from the electric field solution at the molecule locations. This allows one to derive absorption, fluorescence, or Raman/SERS cross-sections<sup>7,30</sup> and molecule orientation effects can be investigated, for example surface selection rules in SERS.<sup>31,32</sup> The main shortcoming of this approach is that, as the molecular response is excluded from the electromagnetic (EM) simulation, it cannot account for effects related to

molecule/molecule interaction (surface coverage dependence) and more importantly for the effect of the adsorbed molecules on the plasmon resonance.

The most common approach to overcome these limitations is to consider the molecular layer as a thin homogeneous medium and to solve Maxwell's equations for the core-shell system.<sup>12,15,23,27–29,33–35</sup> This approach can for example predict the influence of a molecular resonance on the NP's plasmon resonance.<sup>13</sup> One of the difficulties is to relate the properties (e.g. dielectric function) of this macroscopic effective medium to the microscopic properties (e.g. polarizability tensor) of the adsorbate.<sup>36</sup> Often, a simple empirical Lorentz oscillator is assumed but it does not account for any dependence on molecular orientation or coverage, which have been shown to be important<sup>17,26,37</sup>. Very recently, we have developed an accurate model for the anisotropic dielectric tensor of adsorbed molecules treated as an effective layer, which we will refer to as the effective layer model (ELM).<sup>38</sup> This new approach accounts for both molecular concentration and orientation and was validated by comparing it to a microscopic model in the special case of spherical NPs, where extensions of Mie theory can be used to solve Maxwell's equations in the presence of point dipoles representing anisotropic molecules.<sup>26</sup>

In this study, we exploit this model to tackle two outstanding questions in the theory of molecule/plasmon interactions. Firstly, *does molecular orientation affect the adsorbate-induced shift in plasmon resonance?* For this, we first follow Ref.<sup>38</sup> and use anisotropic Mie theory<sup>39</sup> to understand orientation effects on spherical NPs. As plasmon resonances also exhibit anisotropic properties in non-spherical particles, we then extend this study to spheroidal NPs to investigate the interplay between

---

\* tang.chhayly@yahoo.co.nz

† eric.leru@vuw.ac.nz

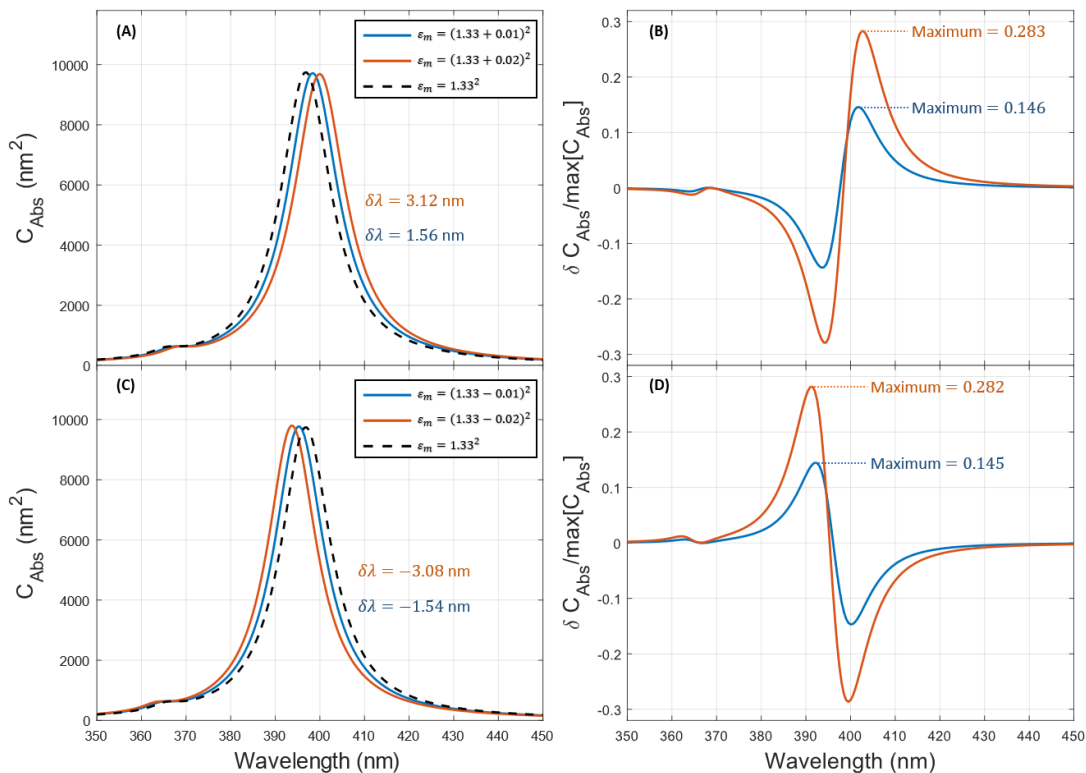


FIG. 1. Absorption cross-section spectra  $C_{\text{abs}}(\lambda)$  for a silver sphere of radius  $a = 14$  nm embedded in a medium of dielectric function  $\varepsilon_m + \delta\varepsilon_m$ , where  $\delta\varepsilon_m$  is a small positive (A) or negative (C) deviation to highlight the refractive index dependence of the plasmon resonance peak. The PR shifts are more evident in the difference spectra (B,D),  $\delta C_{\text{abs}} = C_{\text{abs}}(\varepsilon_m + \delta\varepsilon_m) - C_{\text{abs}}(\varepsilon_m)$ . The magnitude of the PR shift is directly proportional to the amplitude of the normalized difference spectrum: here  $\delta\lambda \approx 10.5 \times \max[\delta C_{\text{abs}}] / \max(C_{\text{abs}})$ .

molecular and plasmonic anisotropy. For this, we chose Finite Element Modelling (FEM) as a convenient method to solve the EM problem in the presence of anisotropic media. We follow the detailed implementation of FEM in COMSOL for plasmonic nanoparticles presented in Ref.<sup>40</sup> and extend it to the case of core/shell systems with anisotropic media. This FEM implementation moreover opens up the way to study non-conventional geometries, which allows us to address the second question: *does the location of the adsorbed molecules affect the adsorbate-induced shift in plasmon resonance?* For this, we consider partial shells with the adsorbate covering only part of the particle surface, e.g. the “hotspot” or the “side”. Such configurations are particularly relevant to experiments exploiting selective adsorption at hot-spots<sup>41–43</sup> or those with special types of NPs whose surface has more than one distinct physical properties, known as “Janus” particles.<sup>44,45</sup>

## I. MOLECULAR ORIENTATION EFFECTS IN SPHERICAL CORE-SHELL SYSTEM

We consider a metallic nanoparticle with isotropic dielectric function  $\varepsilon(\lambda)$  embedded in a non absorbing

isotropic medium of refractive index  $n_m$  and dielectric function  $\varepsilon_m = n_m^2 \geq 1$ . For illustration purposes, we will choose silver NPs with a dielectric function as given in Ref.<sup>7,46</sup> embedded in water with  $n_m = 1.33$ .

### A. Isotropic case

Previous studies have shown that the peak position ( $\lambda_{\text{PR}}$ ) of the plasmon resonance for metallic nanoparticles depends on the refractive index of the surrounding medium,<sup>47</sup> with a higher  $n_m$  resulting in a redshift. The embedding medium effect is illustrated in Fig. 1 using standard Mie theory (no shell). For small changes in refractive index ( $\delta n_m$ ), the PR shift is approximately proportional to  $\delta n_m$ :  $\delta\lambda / \delta n_m \approx 155$  nm/RIU (RIU  $\equiv$  refractive-index-unit) in the example of Fig. 1(A,C). This shift is more evident in the differential spectra where a clear derivative spectral shape is obtained (B,D). Moreover, once normalized by the peak cross-section, the maximum of the difference spectrum is simply proportional to the PR shift. Explicitly, in the example of Fig. 1:  $\delta\lambda \approx 10.5 \times \max[\delta C_{\text{abs}}] / \max(C_{\text{abs}})$ . Difference spectra like shown in Fig. 1(B,D) will therefore be used in the rest of this study to quantify the magnitude of the PR

shift as they provide a much clearer picture in the case of very small shifts and also align more closely with the experimental approach.

A similar effect can be expected from a thin layer of adsorbate on the surface.<sup>13</sup> This can be simply explored within an isotropic core-shell model. The effective dielectric function of the adsorbate shell can be expressed in terms of the polarizability of the molecules  $\alpha_d$  as<sup>38</sup>:

$$\varepsilon_{\text{iso}} = \varepsilon_m + \frac{L_m^2 c_d \alpha_d / \varepsilon_0}{1 - (L_m^2 / \varepsilon_m) c_d \alpha_d / (3\varepsilon_0)} \quad (1)$$

where  $L_m = (\varepsilon_m + 2)/3$  is the local field correction factor,<sup>7,48</sup> and  $c_d$  is the adsorbate concentration in the shell. For a coverage  $\rho$  (in molecule per unit area) and a small shell thickness  $L_s$ ,  $c_d \approx \rho/L_s$ . Intuitively, the shift in the plasmon resonance should then depend on whether  $\Re\{\varepsilon_{\text{iso}}(\lambda_{\text{PR}})\}$  at the plasmon resonance is larger (redshift) or smaller (blueshift) than  $\varepsilon_m$ . Therefore, the polarizability of the adsorbed molecules at the plasmon resonance determines the adsorbate-induced shift. If the two resonances do not overlap and assuming  $\Im\{\alpha_d\} \ll \Re\{\alpha_d\}$ , we can moreover deduce from Eq. 1 the following conditions:

- If  $\Re\{\alpha_d(\lambda_{\text{PR}})\} = 0$ , then there will not be any shift in the plasmon resonance at all.
- If  $0 < \Re\{\alpha_d(\lambda_{\text{PR}})\} < 3\varepsilon_0\varepsilon_m/(L_m^2 c_d)$ , the plasmon resonance will be red-shifted.
- And if  $\Re\{\alpha_d(\lambda_{\text{PR}})\} < 0$  or  $\Re\{\alpha_d(\lambda_{\text{PR}})\} > 3\varepsilon_0\varepsilon_m/(L_m^2 c_d)$ , a blue-shift will be observed. The latter condition is a consequence of molecule/molecule interactions in the adsorbate layer affecting its optical properties and only occurs at very high coverage (large  $c_d$ ).

To illustrate these conditions, we consider a polarizability representative of the dye molecule Rhodamine 6G with a main uniaxial electronic resonance at 526 nm:<sup>48</sup>

$$\alpha_{\text{uni}}(\lambda) = \alpha_\infty - \frac{\alpha_1 \lambda_1}{\mu_1} \left[ 1 - \frac{1}{1 - \frac{\lambda_1^2}{\lambda^2} - i \frac{\lambda_1}{\lambda \mu_1}} \right], \quad (2)$$

where

$$\begin{aligned} \alpha_\infty &= 9.4 \times 10^{-39} \text{ [SI]}, & \lambda_1 &= 526 \text{ nm}, \\ \alpha_1 &= 5.76 \times 10^{-38} \text{ [SI]}, & \mu_1 &= 10000 \text{ nm}. \end{aligned} \quad (3)$$

To model an equivalent isotropic response, we then choose<sup>48</sup>  $\alpha_d = \alpha_{\text{uni}}/3$ . With these parameters and for low dye-coverage  $\rho = 0.01 \text{ nm}^{-2}$ , the second condition is satisfied and a red-shift in the plasmon resonance is predicted, as shown in Fig. 2. From the same relation as obtained in Fig. 1, the PR-shift can be quantified: it is of the order of 0.011 nm or  $4.5 \times 10^{-4} \text{ nm/molecule}$ . We can moreover artificially change the molecule polarizability by changing for example the parameter  $\alpha_1$ , in order to satisfy the other conditions, and we then obtain a blueshift for  $\Re\{\alpha_d(\lambda_{\text{PR}})\} < 0$  and no shift if

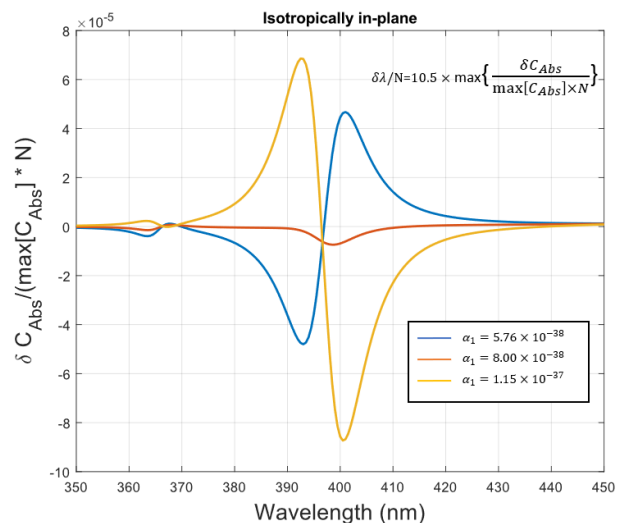


FIG. 2. Differential absorption cross-section,  $\delta C_{\text{abs}}$ , of a 14 nm radius silver sphere in water coated with a thin shell of adsorbate described by Eqs. 1-3.  $\delta C_{\text{abs}}$  is here obtained by subtracting the core-only solution from the core-shell cross-section. This is then normalized by the peak absorption as in Fig. 1(B,D) and the number of adsorbed molecules,  $N$ : here  $\rho = 0.01 \text{ nm}^{-2}$  giving  $N \approx 25$  molecules. Depending on the value of the parameter  $\alpha_1$ , a red-shift, no shift, or blue-shift in the PR peak is predicted. The PR shift per molecule  $\delta\lambda/N$  is related to the observed amplitude as in Fig. 1(B,D).

$\Re\{\alpha_d(\lambda_{\text{PR}})\} \approx 0$  (Fig. 2). In the latter case, there is a very small decrease in the magnitude of the NP resonance. Note also that the quadrupole plasmon resonance (at  $\sim 368 \text{ nm}$ ) is also subject to small shifts, but  $\Re\{\alpha_d\}$  is different there than at the main resonance.

## B. Orientation effects

The isotropic case discussed so far, although not previously quantitatively linked to the molecular polarizabilities, has been well studied. However, many adsorbates have an anisotropic polarizability tensor and a preferred orientation on the surface (i.e. normal, parallel, or at a preferred angle). This should introduce a strong anisotropy in the adsorbate layer response. As shown in Ref.<sup>38</sup>, this can still be treated within the effective layer model, but with an anisotropic dielectric tensor. The simplest case that is still relevant to many experimental situations is when the dielectric tensor is diagonal in the local basis (determined by the surface normal):

$$\underline{\varepsilon} = \begin{pmatrix} \varepsilon_n & 0 & 0 \\ 0 & \varepsilon_t & 0 \\ 0 & 0 & \varepsilon_t \end{pmatrix}. \quad (4)$$

This applies for example to many dyes whose polarizability tensor is uniaxial with a single component  $\alpha_{\text{uni}}(\lambda)$  and with a preferred adsorption orientation. We will here

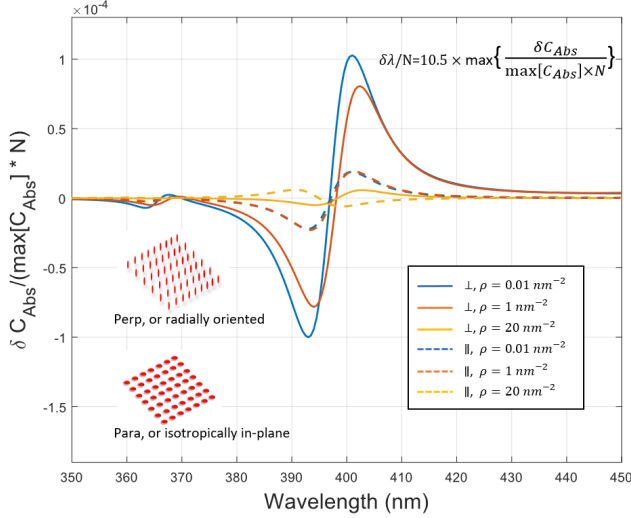


FIG. 3. Normalized differential absorption cross-section per molecule for the two different orientations of adsorbate: perpendicular to the surface ( $\perp$ ) and isotropically in-plane ( $\parallel$ ). Different molecular coverage  $\rho$  are considered. As in previous figures, the PR shift per molecule can be inferred from the maximum of these difference spectra.

consider the two important cases of adsorption where the main polarizability axis is perpendicular ( $\perp$ ) or parallel ( $\parallel$ ) to the surface. In the latter case, the in-plane orientation remains random. The effective dielectric tensor in these two cases is then given by:<sup>38</sup>

$$\begin{aligned} \epsilon_t^\perp &= 0 \\ \frac{1}{\epsilon_n^\perp} &= \frac{1}{\epsilon_m} - \frac{(L_m^2/\epsilon_m^2)c_d\alpha_{\text{uni}}/\epsilon_0}{1 + \frac{\alpha_{\text{uni}}}{4\pi\epsilon_0} \frac{L_m^2}{\epsilon_m} \rho^{3/2}\xi_0}. \end{aligned} \quad (5)$$

and

$$\begin{aligned} \epsilon_t^\parallel &= \epsilon_m + \frac{L_m^2 c_d \alpha_{\text{uni}} / (2\epsilon_0)}{1 - \frac{\alpha_{\text{uni}}}{16\pi\epsilon_0} \frac{L_m^2}{\epsilon_m} \rho^{3/2}\xi_0/2}, \\ \epsilon_n &= 0. \end{aligned} \quad (6)$$

where  $\xi_0 \approx 9.03$  is a constant and  $\rho$  is the surface coverage. We have omitted for simplicity the image-dipole contribution, which could become important when the adsorbate is very close to the surface (typically  $\sim 0.5$  nm),<sup>38</sup> but it does not affect any of our conclusions. In the simplest case of a spherical NP, the EM solution of the isotropic core/anisotropic shell system can be found using an extension of Mie theory to anisotropic media<sup>39,49,50</sup> and some representative results are shown in Fig. 3 for a dye with  $\alpha_{\text{uni}}(\lambda)$  given by Eq. 3. The most striking result is that at low and intermediate concentrations, the amplitude of the adsorbate-induced shift strongly depends on orientation, and is about 5 times larger for perpendicular compared to parallel orientation. As the concentration increases, the denominators become more important, which affects the amplitude of the shift

per molecule, but in a good approximation, the shift remains proportional to the number of molecules up to  $\sim 1$  nm<sup>-2</sup>. At very high concentrations ( $\rho > 12$  nm<sup>-2</sup>), the shift per molecule is much smaller and for in-plane orientation the shift changes to a blueshift as discussed earlier. Note that at such a high concentration, dyes would most likely form H- or J-aggregates.

Comparing the results of Fig. 3 to the isotropic case (Fig. 2), it appears that the PR shift per molecule is around 2.5 times larger for perpendicular molecules than for equivalent isotropic or randomly-oriented molecules. In fact, it is dominated by the perpendicular component of the polarizability tensor in the latter case. We can therefore expect a comparable enhancement (a factor of 2.5) of the LSPR sensitivity, which should exceed theoretical limits derived for isotropic adsorbates.<sup>22,24,25</sup>

It is not clear *a priori* what is causing the difference in adsorbate-induced shift with orientation. The molecules are experiencing very different electric fields for different orientation (with plasmonic field enhancements always much larger for the perpendicular direction), which likely contributes to the discrepancy as previously suggested in the isotropic case.<sup>22,24,25</sup> In order to further investigate this aspect, we can consider non-spherical NP, which allows us to further tune the plasmonic field enhancements by changing the aspect ratio.

## II. MOLECULAR ORIENTATION EFFECTS IN SPHEROIDAL CORE-SHELL SYSTEM

For simplicity, we will focus specifically on spheroidal NPs. The  $T$ -matrix method then provides an accurate solution of the EM problem,<sup>51-53</sup> which can be extended to isotropic core-shell systems.<sup>54</sup> There is however no extension to anisotropic shells and we therefore have to resort to a fully numerical scheme. Finite Element Modelling (FEM) has proven very efficient and accurate for plasmonic NPs<sup>40,55-57</sup> and has the versatility to model core-shell systems and incorporate anisotropic dielectric tensors. We therefore developed an implementation of the effective anisotropic dielectric tensor in FEM using COMSOL, the details of which are given in the methods section. Note that this implementation was validated against the exact anisotropic Mie theory solution in the special case of spheres.

We have used these FEM simulations to investigate the optical properties of adsorbed molecules, modeled as an anisotropic spheroidal shell, around a silver prolate spheroidal NP of aspect ratio 3. The results are shown in Fig. 4. With incident polarization along the long axis of the spheroid, the main dipolar resonance at  $\sim 660$  nm is excited. This also creates a strong localized hot-spot at the tip, where the enhanced electric field is primarily perpendicular to the surface.<sup>7,58</sup> This can be quantified explicitly by calculating the surface-averaged perpendicular and parallel components of the local field

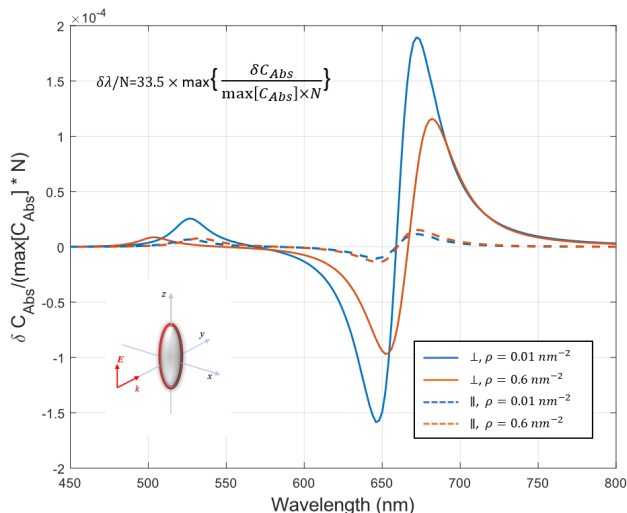


FIG. 4. FEM predictions of the normalized differential absorption cross-section per molecule for an anisotropic layer of dye-molecules ( $\perp$  or  $\parallel$ , as in Fig. 3) around a silver prolate spheroid ( $29 \times 87$  nm) embedded in water. The incident polarization is along the long axis and excites the main dipolar plasmon resonance at 660 nm. The PR shift  $\delta\lambda$  can be deduced from the differential spectrum as before, but with a different proportionality coefficient as the resonance is different to that of the sphere.

intensity enhancement factor (EF):

$$M^{\perp} = \langle |E_n|^2 \rangle \quad (7)$$

$$M^{\parallel} = \frac{1}{2} [\langle |E_t|^2 + |E_u|^2 \rangle] \quad (8)$$

where  $(n, t, u)$  refer to the local coordinate system with  $n$  indicating the normal component. The factor  $1/2$  in the second equation is included to account for the in-plane orientation averaging for uniaxial molecules. For the example of Fig. 4,  $T$ -matrix calculations<sup>53</sup> give at the plasmon resonance:  $M^{\perp} \approx 956$  and  $M^{\parallel} \approx 63$ , i.e. a ratio of  $\sim 15$ . In comparison, for the sphere, we had  $M^{\perp} \approx 633$  and  $M^{\parallel} \approx 133$ , i.e. a smaller ratio of  $\sim 5$ . This appears to translate into a larger discrepancy in the induced PR shift between  $\perp$  and  $\parallel$  cases, with a factor of  $\sim 16$  here compared to  $\sim 5$  for the sphere. The ratio  $\perp/\parallel$  for the PR shifts appear to be approximately the same as the ratio for surface-average field EF. In absolute terms, the PR shift per molecule is  $\sim 0.0062$  nm for  $\perp$  orientation on the spheroid, about 5 times more than for the sphere case. Some of this increase sensitivity can be explained by the shift of the resonance to longer wavelength, which should increase the maximum sensitivity by the ratio of plasmon resonance wavelength,<sup>22</sup>  $\sim 1.65$ . The remainder (a factor of 3) does not quite correlate as quantitatively with the change in  $M^{\perp}$  (from 633 for the sphere to 956 for the spheroid), so there may be an additional geometric effect enhancing the PR shift in elongated NPs. These observations nevertheless confirm our earlier speculation that the amplitude of the PR shift is correlated

TABLE I. Summary of the predicted PR shifts per molecule  $\delta\lambda/N$  [nm] for the partial shell calculations shown in Fig. 5.

		$\delta\lambda/N$ [ $10^{-4}$ nm]		$\langle  E ^2 \rangle$	
		Caps	Donut	Caps	Donut
$E_z, k_x$	$\perp$	33.3	2.30	1630	454
	$\parallel$	0.54	0.99	29	152
$E_x, k_z$	$\perp$	3.12	3.64	135	722
	$\parallel$	3.65	0.80	184	124

with the local field enhancement experienced by the adsorbate along its optical axis. In this context, the larger shifts for  $\perp$  orientation can be viewed as a consequence of the larger average enhancement perpendicular to the metal surface. This interpretation is consistent with earlier theoretical work in the isotropic case demonstrating the importance of local field enhancements to quantify the PR shifts.<sup>22,24,25</sup>

### III. MOLECULAR POSITION EFFECTS

The FEM implementation of the anisotropic effective layer model allows us to solve a wide class of problems. We can in particular investigate how the adsorbate location on the surface may influence its effect on the plasmon resonance shift. Almost all theoretical studies assume a uniform coverage on the surface, but we here instead consider spherical NPs partially coated with anisotropic molecules (non-spherical particles could also be easily implemented but are not considered here). From our discussion so far, one could expect that molecules located at a hotspot would result in larger shifts than those located in regions of lowest field enhancement. Two cases are studied here: spherical caps, and its complementary structure: the “donut shell” (Fig. 5). The half-angle of the cone defining the spherical caps is  $32^\circ$ , so the total surface area of the two caps is  $\sim 15\%$  and that of the donut is  $85\%$  ( $\sim 5.7$  times larger). At equivalent coverage, the donut therefore contains almost six times more adsorbed molecules.

The results from the two types of partial shells are summarized in Fig. 5(A,C) for two types of incident polarizations. We again consider both types of orientation of the uniaxial adsorbed molecules (in-plane and perpendicular). For direct comparison, we also calculate the surface-averaged field EFs,  $M^{\perp}$  and  $M^{\parallel}$  for the entire sphere, for the caps, and for the donut, see Fig. 5(B,D). To make it easier to compare these results, the average field enhancements at resonance and PR shifts per molecule are summarized in Table I.

For  $E_z$  excitation, EM hot-spots are formed at the caps and the average perpendicular field enhancement at resonance is  $\sim 60$  times larger than for parallel. This translates into an equally larger induced PR shift per molecule, by a factor  $\sim 60$ , much larger than observed for the full shell (which was a factor of  $\sim 5$ ). This again

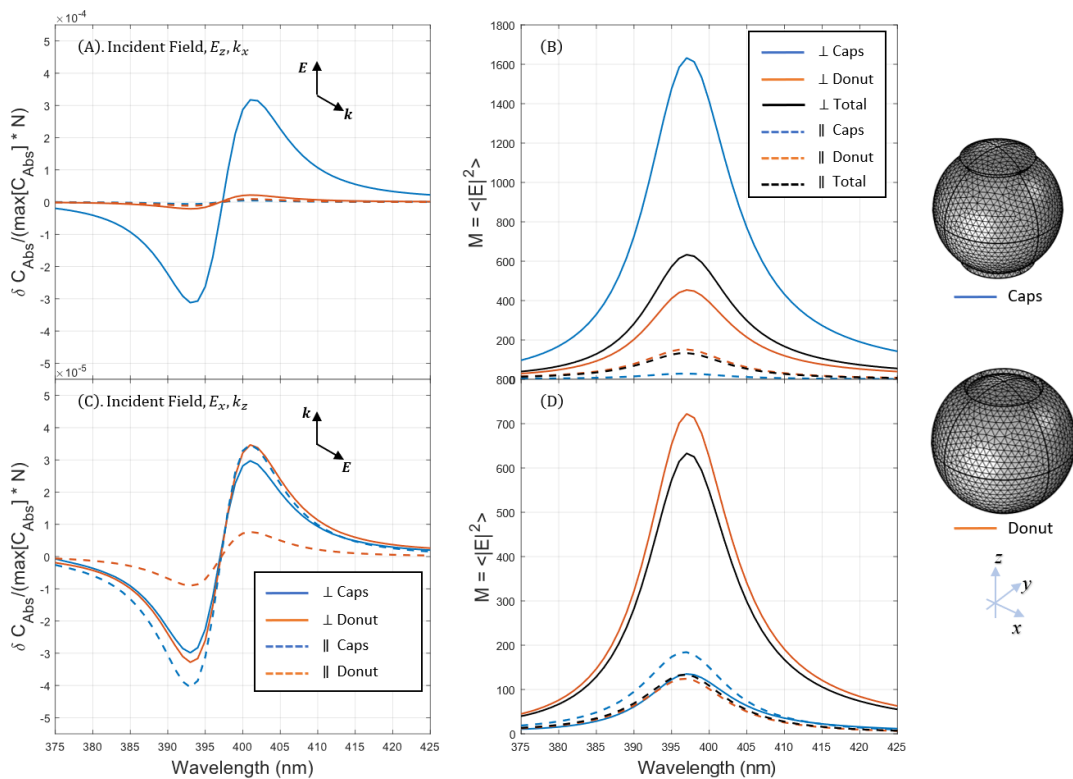


FIG. 5. Normalized differential absorption cross-section per molecule for partial shells around a 14 nm radius silver sphere in water. We consider the two partial shells shown on the right and called caps and donuts, two orientations ( $\perp$  and  $\parallel$ ), and two incident excitations:  $E_z, k_x$  (A,B) and  $E_x, k_z$  (C,D). The corresponding surface-averaged field EF,  $M^\perp$  and  $M^\parallel$  in the caps, donut, and full sphere are shown on the right (B,D). The surface coverage is  $\rho = 0.6 \text{ nm}^{-2}$ .

supports the conclusion that the field enhancement along the molecular axis and PR shifts are strongly correlated. The same strong correlation is observed when comparing perpendicular and parallel cases for the donut and for both partial shells with the other incident polarization along  $E_x$ . Comparing the  $E_z$  and  $E_x$  excitation, it also appears that the PR shift scales with the average field EF. This strong quantitative correlation is only lost when comparing the caps and the donut. For example, the PR shift per molecule for  $E_z$  polarization and  $\perp$  orientation is  $\sim 15$  times larger in the cap than in the donut, but the average LFEF is only  $\sim 3.6$  larger. The same discrepancy, by a factor  $\sim 4$ , is also evident for other configurations. It is not clear why this is, but has perhaps the same origin as the discrepancy observed when comparing the sphere and spheroid cases.

To summarize these findings, the PR shift per molecule appears to be quantitatively proportional to the average field EF along the main molecular axis, especially when considering relative shifts between  $\perp$  and  $\parallel$  orientation, or between  $E_z$  and  $E_x$  polarization. In addition, the PR shift per molecule at the hot-spot can be much larger than on average for a full shell, here by a factor  $\sim 3$  for a sphere. Given our earlier discussion of spheroidal NPs, even larger enhancements can be expected for molecules adsorbed perpendicular to the surface at the tips of an

elongated NP.

#### IV. DISCUSSION AND CONCLUSION

In this work, we have clearly demonstrated the importance of molecular orientation and position in determining the adsorbate-induced shifts in the plasmon resonance of nanoparticles. Molecules adsorbed with their main optical axis perpendicular to the surface can induce much larger shifts. Molecules located at the EM hot-spots contribute much more than the others. These two observations can be simply explained by the fact that the resonance shift appears to be strongly correlated with the local field enhancements experienced by the molecules.

These findings, which cannot be deduced from existing isotropic core-shell models, have important implications for LSPR sensing and can be used to engineer LSPR sensors with greatly enhanced sensitivity, likely well above the isotropic theoretical limits.<sup>22,24,25</sup> For example, a spheroidal nanoparticle that selectively captures a target analyte only at its tips and with a perpendicular orientation would result in PR shifts one or two orders of magnitude larger than a standard sensor, with a comparable improvement in sensitivity. We hope this work will pave the way for the development of such high-sensitivity

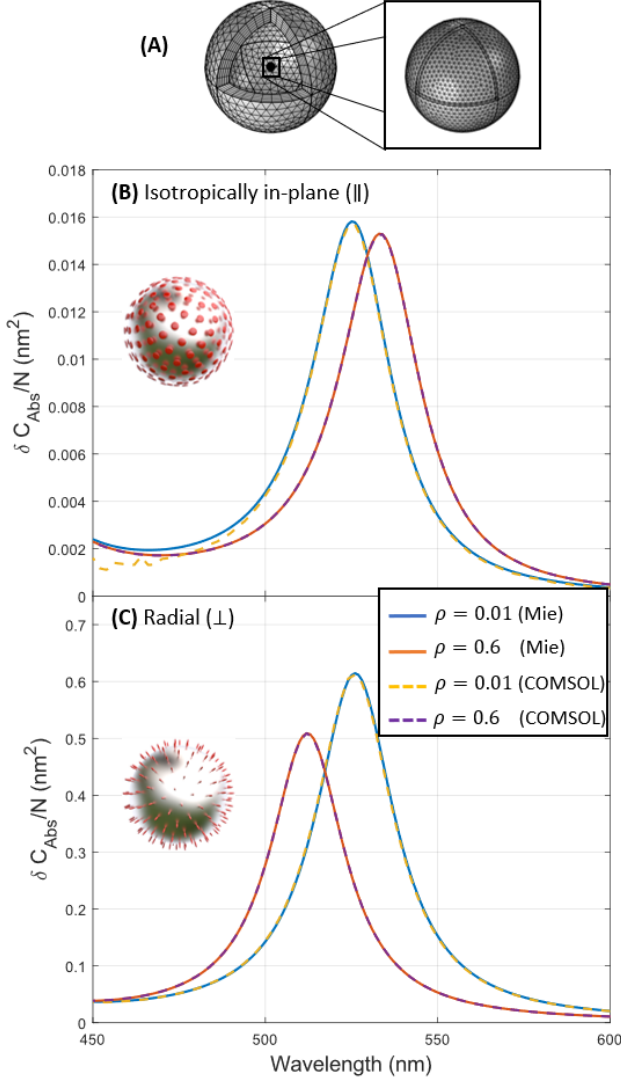


FIG. 6. FEM calculations with anisotropic dielectric tensor. (A) Geometry of the problem and grid mesh: spherical PML on the left and the coated nanoparticle zoomed-in on the right. (B,C) Comparison between FEM (COMSOL simulations) and Mie theory results for a 14 nm silver sphere embedded in water and coated with an anisotropic layer of molecules (following Eqs. 2-6). The results show the wavelength dependence of the differential absorption cross-section (normalized by the number of molecules) around the molecular resonance for isotropically in-plane (B) and perpendicular (C) orientations for two different coverages.

LSPR sensors.

## METHODS

**FEM of core-shell structures with anisotropic effective dielectric tensors.** The finite-element method (FEM)<sup>59,60</sup> can be used to solve the Helmholtz equation (or Maxwell's equations) in the frequency

domain and has been applied to metallic nanostructures for plasmonics.<sup>40,55,56</sup> As a general numerical differential equation solver, it can in principle apply to arbitrary shaped, dispersive, inhomogeneous, and anisotropic structures. A grid mesh (typically triangular on surfaces and tetrahedral on volumes) is used to discretize the geometry. The mesh can be chosen to be denser for regions with fine structure. One crucial point in the FEM approach is to avoid the reflection of the incident or scattered fields at the boundary of the computational domain, which could result in an inaccurate solution. Perfectly matched layers (PML) are one of the most efficient approaches to achieve this, providing that they are sufficiently meshed. Ref.<sup>40</sup> provides a detailed description of PML setting and grid mesh considerations using COMSOL and showed that very accurate results can be obtained for metallic NPs. We here follow this implementation and add a shell layer (Fig.6(A)), with the only additional complication being the anisotropic dielectric tensor.

**Dielectric tensor for spherical shell.** In order to define the anisotropic dielectric tensor in the shell in COMSOL, we need to describe it in the Cartesian basis, instead of the local basis defined by the surface normal (as given in Eq. 4). This dielectric tensor can be transformed into the Cartesian basis by using the transformation:

$$\underline{\epsilon}_{\text{Cart}} = \mathcal{S}^T \cdot \underline{\epsilon} \cdot \mathcal{S}, \quad (9)$$

where  $\mathcal{S}$  is the transformation matrix from Cartesian to Local coordinates (with  $\mathcal{S}^{-1} = \mathcal{S}^T$ ). The latter depends on the NP geometry, so we have implemented it only on specific geometries. For the sphere, we simply have:

$$\mathcal{S}_{\text{Sphere}} = \begin{bmatrix} \sin \theta \cos \phi & \sin \theta \sin \phi & \cos \theta \\ \cos \theta \cos \phi & \cos \theta \sin \phi & -\sin \theta \\ -\sin \phi & \cos \phi & 0 \end{bmatrix}. \quad (10)$$

where  $(r, \theta, \phi)$  are the spherical coordinates.

**Dielectric tensor for spheroidal shell.** For the spheroid, the surface can be parametrized by two angles,  $\alpha, \beta$ , as:

$$\begin{aligned} x &= a \sin \alpha \cos \beta, \\ y &= a \sin \alpha \sin \beta, \\ z &= c \cos \alpha. \end{aligned} \quad (11)$$

with  $a < c$  (prolate) or  $a > c$  (oblate).

The normal (but not unit norm) vector can then be derived as:

$$\mathbf{N} = \frac{\sin \alpha \cos \beta}{a} \hat{\mathbf{x}} + \frac{\sin \alpha \sin \beta}{a} \hat{\mathbf{y}} + \frac{\cos \alpha}{c} \hat{\mathbf{z}}, \quad (12)$$

We then find two orthogonal tangential vectors (again not normalized to unit norm):

$$\begin{aligned} \mathbf{T} &= a \cos \alpha \cos \beta \hat{\mathbf{x}} + a \cos \alpha \sin \beta \hat{\mathbf{y}} - c \sin \alpha \hat{\mathbf{z}} \\ \mathbf{U} &= -a \sin \alpha \sin \beta \hat{\mathbf{x}} + a \sin \alpha \cos \beta \hat{\mathbf{y}}. \end{aligned} \quad (13)$$

$(\mathbf{N}/|\mathbf{N}|, \mathbf{T}/|\mathbf{T}|, \mathbf{U}/|\mathbf{U}|)$  is a local basis of the surface. The

transformation matrix for a spheroidal NP is then given by:

$$\mathcal{S}_{\text{Spheroid}} = \begin{bmatrix} |\mathbf{N}|^{-1} \sin \alpha \cos \beta/a & |\mathbf{N}|^{-1} \sin \alpha \sin \beta/a & |\mathbf{N}|^{-1} \cos \alpha/c \\ |\mathbf{T}|^{-1} a \cos \alpha \cos \beta & |\mathbf{T}|^{-1} a \cos \alpha \sin \beta & -|\mathbf{T}|^{-1} c \cos \alpha \cos \beta \\ -|\mathbf{U}|^{-1} a \sin \alpha \sin \beta & |\mathbf{U}|^{-1} a \sin \alpha \cos \beta & 0 \end{bmatrix}. \quad (14)$$

**Validation.** The validity of the FEM calculations was verified for a silver sphere in water against the anisotropic Mie theory solution as shown in Fig. 6.

Grant of the Royal Society New Zealand (ECLR).

### ACKNOWLEDGMENTS

The authors acknowledge financial support from a Rutherford Discovery Fellowship (BA) and a Marsden

- 
- [1] K. A. Willets and R. P. Van Duyne, Localized surface plasmon resonance spectroscopy and sensing, *Annu. Rev. Phys. Chem.* **58**, 267 (2007).
- [2] P. Englebienne, Use of colloidal gold surface plasmon resonance peak shift to infer affinity constants from the interactions between protein antigens and antibodies specific for single or multiple epitopes, *Analyst* **123**, 1599 (1998).
- [3] M. D. Malinsky, K. L. Kelly, G. C. Schatz, and R. P. Van Duyne, Chain length dependence and sensing capabilities of the localized surface plasmon resonance of silver nanoparticles chemically modified with alkanethiol self-assembled monolayers, *J. Am. Chem. Soc.* **123**, 1471 (2001).
- [4] A. J. Haes and R. P. Van Duyne, A nanoscale optical biosensor: Sensitivity and selectivity of an approach based on the localized surface plasmon resonance spectroscopy of triangular silver nanoparticles, *J. Am. Chem. Soc.* **124**, 10596 (2002).
- [5] N. Nath and A. Chilkoti, A colorimetric gold nanoparticle sensor to interrogate biomolecular interactions in real time on a surface, *Anal. Chem.* **74**, 504 (2002).
- [6] A. D. McFarland and R. P. Van Duyne, Single silver nanoparticles as real-time optical sensors with zeptomole sensitivity, *Nano Lett.* **3**, 1057 (2003).
- [7] E. C. Le Ru and P. G. Etchegoin, *Principles of Surface-Enhanced Raman Spectroscopy: and Related Plasmonic Effects* (Elsevier, 2009).
- [8] M. Moskovits, Surface-enhanced spectroscopy, *Rev. Mod. Phys.* **57**, 783 (1985).
- [9] C. D. Geddes and J. R. Lakowicz, Metal-enhanced fluorescence, *J. Fluorescence* **12**, 121 (2002).
- [10] E. C. Le Ru, P. G. Etchegoin, J. Grand, N. Féliidj, J. Aubard, and G. Lévi, The mechanisms of spectral profile modification in surface enhanced fluorescence, *J. Phys. Chem. C* **111**, 16076 (2007).
- [11] C. M. Galloway, P. G. Etchegoin, and E. C. Le Ru, Ultrafast nonradiative decay rates on metallic surfaces by comparing surface-enhanced Raman and fluorescence signals of single molecules, *Phys. Rev. Lett.* **103**, 063003 (2009).
- [12] G. P. Wiederrecht, G. A. Wurtz, and J. Hranisavljevic, Coherent coupling of molecular excitons to electronic polarizations of noble metal nanoparticles, *Nano Lett.* **4**, 2121 (2004).
- [13] J. Zhao, L. Jensen, J. Sung, S. Zou, G. C. Schatz, and R. P. Van Duyne, Interaction of plasmon and molecular resonances for rhodamine 6G adsorbed on silver nanoparticles, *J. Am. Chem. Soc.* **129**, 7647 (2007).
- [14] J. Yan, W. Zhang, S. Duan, X. Zhao, and A. O. Govorov, Optical properties of coupled metal-semiconductor and metal-molecule nanocrystal complexes: Role of multipole effects, *Phys. Rev. B* **77**, 165301 (2008).
- [15] N. T. Fofang, T. Park, O. Neumann, N. A. Mirin, P. Nordlander, and N. J. Halas, Plexcitonic nanoparticles: Plasmon-exciton coupling in nanoshell-J-aggregate complexes, *Nano Lett.* **8**, 3481 (2008).
- [16] W. Ni, H. Chen, J. Su, Z. Sun, J. Wang, and H. Wu, Effects of dyes, gold nanocrystals, pH, and metal ions on plasmonic and molecular resonance coupling, *J. Am. Chem. Soc.* **132**, 4806 (2010).
- [17] B. L. Darby, B. Auguie, M. Meyer, A. E. Pantoja, and E. C. Le Ru, Modified optical absorption of molecules on metallic nanoparticles at sub-monolayer coverage, *Nat. Photonics* **10**, 40 (2016).
- [18] A. M. Fales, S. J. Norton, B. M. Crawford, B. G. DeLacy, and T. Vo-Dinh, Fano resonance in a gold nanosphere with a J-aggregate coating, *Phys. Chem. Chem. Phys.* **17**, 24931 (2015).
- [19] R. Chikkaraddy, B. de Nijs, F. Benz, S. J. Barrow, O. A. Scherman, E. Rosta, A. Demetriadou, P. Fox, O. Hess, and J. J. Baumberg, Single-molecule strong coupling at room temperature in plasmonic nanocavities, *Nature* **535**, 127 (2016).

- [20] G. Zengin, T. Gschneidner, R. Verre, L. Shao, T. J. Antosiewicz, K. Moth-Poulsen, M. Käll, and T. Shegai, Evaluating conditions for strong coupling between nanoparticle plasmons and organic dyes using scattering and absorption spectroscopy, *J. Phys. Chem. C* **120**, 20588 (2016).
- [21] T. E. Tesema, H. Kookhaee, and T. G. Habteyes, Extracting electronic transition bands of adsorbates from molecule-plasmon excitation coupling, *J. Phys. Chem. Lett.* **11**, 3507 (2020).
- [22] S. J. Zalyubovskiy, M. Bogdanova, A. Deinega, Y. Lozovik, A. D. Pris, K. H. An, W. P. Hall, and R. A. Potyrailo, Theoretical limit of localized surface plasmon resonance sensitivity to local refractive index change and its comparison to conventional surface plasmon resonance sensor, *J. Opt. Soc. Am. A* **29**, 994 (2012).
- [23] L. Bergamini and S. Corni, Benchmarking common approximations for determining the particle-size dependence of adsorbate-induced localized surface plasmon resonance shifts, *J. Phys. Chem. C* **117**, 14742 (2013).
- [24] W. Zhang and O. J. F. Martin, A universal law for plasmon resonance shift in biosensing, *ACS Photonics* **2**, 144 (2015).
- [25] J. Yang, H. Giessen, and P. Lalanne, Simple analytical expression for the peak-frequency shifts of plasmonic resonances for sensing, *Nano Lett.* **15**, 3439 (2015).
- [26] B. Auguie, B. L. Darby, and E. C. Le Ru, Electromagnetic interactions of dye molecules surrounding a nanosphere, *Nanoscale* **11**, 12177 (2019).
- [27] W. Ni, T. Ambjornsson, S. P. Apell, H. Chen, and J. Wang, Observing plasmonic-molecular resonance coupling on single gold nanorods, *Nano Lett.* **10**, 77 (2010).
- [28] T. J. Antosiewicz, S. P. Apell, and T. Shegai, Plasmon-exciton interactions in a core-shell geometry: from enhanced absorption to strong coupling, *ACS Photonics* **1**, 454 (2014).
- [29] A. O. Cacciola, O. Di Stefano, R. Stassi, R. Saija, and S. Savasta, Ultrastrong coupling of plasmons and excitons in a nanoshell, *ACS Nano* **8**, 11483 (2014).
- [30] E. C. Le Ru and P. G. Etchegoin, Quantifying SERS enhancements, *MRS Bulletin* **38**, 631 (2013).
- [31] M. Moskovits, Surface selection rules, *J. Chem. Phys.* **77**, 4408 (1982).
- [32] E. C. Le Ru, S. A. Meyer, C. Artur, P. G. Etchegoin, J. Grand, P. Lang, and F. Maurel, Experimental demonstration of surface selection rules for SERS on flat metallic surfaces, *Chem. Comm.* **47**, 3903 (2011).
- [33] H. Chen, L. Shao, K. C. Woo, J. Wang, and H.-Q. Lin, Plasmonic-molecular resonance coupling: Plasmonic splitting versus energy transfer, *J. Phys. Chem. C* **116**, 14088 (2012).
- [34] G. Zengin, G. Johansson, P. Johansson, T. J. Antosiewicz, M. Käll, and T. Shegai, Approaching the strong coupling limit in single plasmonic nanorods interacting with J-aggregates, *Sci. Rep.* **3**, 3074 (2013).
- [35] A. E. Schlather, N. Large, A. S. Urban, P. Nordlander, and N. J. Halas, Near-field mediated plexcitonic coupling and giant Rabi splitting in individual metallic dimers, *Nano Lett.* **13**, 3281 (2013).
- [36] D. E. Aspnes, Local-field effects and effective medium theory: a microscopic perspective, *A. J. Phys.* **50**, 704 (1982).
- [37] B. Auguie and E. C. Le Ru, Optical absorption of dye molecules in a spherical shell geometry, *J. Phys. Chem. C* **122**, 19110 (2018).
- [38] C. Tang, B. Auguie, and E. C. Le Ru, Refined effective-medium model for the optical properties of nanoparticles coated with anisotropic molecules, *Phys. Rev. B* **103**, 085436 (2021).
- [39] J. Roth and M. J. Dignam, Scattering and extinction cross sections for a spherical particle coated with an oriented molecular layer, *J. Opt. Soc. Am.* **63**, 308 (1973).
- [40] J. Grand and E. C. Le Ru, Practical implementation of accurate finite-element calculations for electromagnetic scattering by nanoparticles, *Plasmonics* **15**, 109 (2020).
- [41] E. C. Le Ru, J. Grand, I. Sow, W. R. C. Somerville, P. G. Etchegoin, M. Treguer-Delapierre, G. Charron, N. Felidj, G. Levi, and J. Aubard, A scheme for detecting every single target molecule with surface-enhanced Raman spectroscopy, *Nano Lett.* **11**, 5013 (2011).
- [42] A. Lee, G. F. S. Andrade, A. Ahmed, M. L. Souza, N. Coombs, E. Tumarkin, K. Liu, R. Gordon, A. G. Brolo, and E. Kumacheva, Probing dynamic generation of hot-spots in self-assembled chains of gold nanorods by surface-enhanced Raman scattering, *J. Am. Chem. Soc.* **133**, 7563 (2011).
- [43] T. Chen, C. Du, L. H. Tan, Z. Shen, and H. Chen, Site-selective localization of analytes on gold nanorod surface for investigating field enhancement distribution in surface-enhanced Raman scattering, *Nanoscale* **3**, 1575 (2011).
- [44] M. Lattuada and T. A. Hatton, Synthesis, properties and applications of Janus nanoparticles, *Nano Today* **6**, 286 (2011).
- [45] S. J. de Carvalho, R. Metzler, and A. G. Cherstvy, Inverted critical adsorption of polyelectrolytes in confinement, *Soft Matter* **11**, 4430 (2015).
- [46] P. G. Etchegoin, E. C. Le Ru, and M. Meyer, An analytic model for the optical properties of gold, *J. Chem. Phys.* **125**, 164705 (2006).
- [47] T. R. Jensen, M. L. Duval, K. L. Kelly, A. A. Lazarides, G. C. Schatz, and R. P. Van Duyne, Nanosphere lithography: Effect of the external dielectric medium on the surface plasmon resonance spectrum of a periodic array of silver nanoparticles, *J. Phys. Chem. B* **103**, 9846 (1999).
- [48] A. Djorović, M. Meyer, B. L. Darby, and E. C. Le Ru, Accurate modeling of the polarizability of dyes for electromagnetic calculations, *ACS Omega* **2**, 1804 (2017).
- [49] C. Tang, B. Auguie, and E. C. Le Ru, Modeling molecular orientation effects in dye-coated nanostructures using a thin-shell approximation of Mie theory for radially anisotropic media, *ACS Photonics* **5**, 5002 (2018).
- [50] C. Tang, B. Auguie, and E. C. Le Ru, Thin-shell approximation of Mie theory for a thin anisotropic layer spaced away from a spherical core: Application to dye-coated nanostructures, *Phys. Rev. A* **104**, 033502 (2021).
- [51] M. I. Mishchenko, L. D. Travis, and A. A. Lacis, *Scattering, Absorption, and Emission of Light by Small Particles* (Cambridge University Press, 2002).
- [52] W. R. C. Somerville, B. Auguie, and E. C. Le Ru, Accurate and convergent T-matrix calculations of light scattering by spheroids, *J. of Quant. Spectrosc. Rad. Transf.* **160**, 29 (2015).
- [53] W. R. C. Somerville, B. Auguie, and E. C. Le Ru, SMARTIES: User-friendly codes for fast and accurate calculations of light scattering by spheroids, *J. Quant. Spectrosc. Rad. Transf.* **174**, 39 (2016).
- [54] A. Quirantes, A T-matrix method and computer code for

- randomly oriented, axially symmetric coated scatterers, *J. Quant. Spectrosc. Rad. Transf.* **92**, 373 (2005).
- [55] C. G. Khoury, S. J. Norton, and T. Vo-Dinh, Plasmonics of 3-D nanoshell dimers using multipole expansion and finite element method, *ACS Nano* **3**, 2776 (2009).
- [56] C. G. Khoury, S. J. Norton, and T. Vo-Dinh, Investigating the plasmonics of a dipole-excited silver nanoshell: Mie theory versus finite element method, *Nanotechnology* **21**, 315203 (2010).
- [57] M. Kupresak, X. Zheng, G. A. E. Vandenbosch, and V. V. Moshchalkov, Benchmarking of software tools for the characterization of nanoparticles, *Opt. Express* **25**, 26760 (2017).
- [58] E. C. Le Ru and P. G. Etchegoin, Single molecule surfaced-enhanced Raman spectroscopy, *Annu. Rev. Phys. Chem.* **63**, 65 (2012).
- [59] P. Monk, *Finite Element Methods for Maxwell's Equations* (Oxford University Press, 2003).
- [60] J. Jin, *The finite element method in electromagnetics* (John Wiley & Sons, 2015).